Materials Today Bio 32 (2025) 101786

Contents lists available at ScienceDirect

Materials Today Bio

journal homepage: www.journals.elsevier.com/materials-today-bio

3D bioprinted thick hepatic constructs with vascular network as a physiologically relevant *in vitro* organ model

Young-Wook Moon, Timothy Dobroski, Kelsey Willson, Jin-Oh Jeong, Colin Bishop, Anthony Atala, James J. Yoo *, Sang Jin Lee **

Wake Forest Institute for Regenerative Medicine, Wake Forest University School of Medicine, Winston-Salem, NC, 27157, United States

ARTICLE INFO

Keywords:
Bioprinting
Digital light processing (DLP)
Hepatic tissue
Vascularization

ABSTRACT

Establishing adequate vascularization to engineered organs remains a significant challenge that must be addressed. This study presents a novel approach to fabricating viable thick metabolic tissue (>1 cm^3) for applications in human physiology, fundamental biology, and medicine. We designed a tissue construct with a gyroid-shaped architecture to enable uniform flow and surface shear stress that adequately covers the inner surfaces of cell-laden constructs. The constructs (1 × 1 × 1 cm^3) were fabricated using a digital light projection (DLP) printer with a cell-laden poly(ethylene glycol) (PEG)/gelatin methacryloyl (GelMA) bioink combined with human hepatocytes (HepG2), followed by coating the interconnected vascular channels with human endothelial cells (ECs). These constructs were then placed in flow chambers connected to a medium reservoir for continuous perfusion for up to 30 days. The constructs retained their original dimensions, and the cells maintained a greater than 85 % viability at all time points. Immunofluorescent staining confirmed hepatocytes and ECs using cell-specific markers (HNF4-α/albumin for hepatocytes and vWF for ECs). The EC layer effectively lined the vascular lumens, while viable hepatocyte aggregates populated the interior of the constructs. Functional assays demonstrated that the hepatocytes produced albumin and bilirubin at levels comparable to those observed in humans, validating the metabolic functionality of the hepatic tissue constructs. This study successfully developed thick, vascularized human hepatic tissue in an *in vitro* environment, maintaining functionality comparable to native liver cells over 30 days. The innovative gyroid design applied in these organ constructs represents a significant advancement in developing physiologically relevant *in vitro* vascularized organ models.

1. Introduction

Over the past several decades, tissue engineering and regenerative medicine have made remarkable progress, driven by the integration of diverse scientific disciplines [1,2]. Despite these advancements, replicating the intricate architecture and functionality of solid organs remains a significant challenge [3,4]. This difficulty arises from the need to recreate micron-scale functional units with complex vasculature [5,6]. Among these organs, the liver poses unique challenges due to its multifaceted roles in metabolism and detoxification, coupled with its highly complex 3D structure and diverse cellular composition. Numerous engineering strategies have been explored to fabricate functional liver tissue constructs [7]; however, none have achieved significant success in producing thick (larger than 1 cm^3), physiologically relevant liver constructs *in vitro* due to limited vasculature.

In recent years, 3D printing has emerged as a transformative tool to develop advanced technologies for translational applications [1,8–14]. Recognized for its unmatched precision in positioning cells and biomaterials, 3D bioprinting has revolutionized the fabrication of physiologically relevant *in vitro* tissue models [15,16]. Using 3D bioprinting, strategies for creating vascularized tissue constructs have been designed to address the existing challenges of engineered tissues and organs [4]. In particular, 3D printing techniques have been employed to fabricate engineered tissue constructs with intricate microchannel architectures [17]. For instance, sacrificial materials have been extensively investigated for fabricating desired geometric features by encasing a non-sacrificial component within a sacrificial material and removing it [18]. This approach can create a complex network resembling *in vivo*

This article is part of a special issue entitled: Light-based 3D bioprinting applications published in Materials Today Bio.

* Corresponding author.
** Corresponding author.
E-mail addresses: jyoo@wakehealth.edu (J.J. Yoo), sjlee@wakehealth.edu (S.J. Lee).

https://doi.org/10.1016/j.mtbio.2025.101786
Received 31 January 2025; Received in revised form 9 April 2025; Accepted 21 April 2025
Available online 21 April 2025

vasculature in vascular networks [19]. Seeding primary endothelial and perivascular cells into the microchannel structure formed perfusable vascular tubes with endothelial barrier function, similar to native vessels. Despite the enormous potential of 3D printing in achieving vascularization within engineered tissues and organs, several challenges persist. While branched networks [20] or multichannel structures enable constructs to be perfused, regions with insufficient nutrient and oxygen supply remain devoid of blood flow. Overcoming these limitations is crucial for achieving the viability, functionality, and clinical relevance of vascularized tissue constructs.

The gyroid design, initially discovered by mathematician Alan Schoen in 1970 during his NASA research, is renowned for its smooth, continuous, and non-intersecting surfaces [21,22]. This unique geometry makes it an optimal choice for applications requiring efficient material utilization and functionality. The gyroid's structural integrity consists of an interconnected and continuous network of microchannels, facilitating uniform fluid flow throughout the material. We hypothesized that gyroid design-incorporated tissue constructs would maintain cell viability and function through constant perfusion. This construct would provide an optimal environment to support cell viability and sustain cellular functions when cells are integrated into its intricate network of interconnected channels.

In this study, we aimed to develop a fully perfusable hepatic tissue construct ($1 \times 1 \times 1$ cm^3) with a gyroid structure (Fig. 1). The primary objective was to evaluate the construct's viability for more than 30 days *in vitro* while maintaining its hepatic functions, including albumin and bilirubin secretion. To achieve this, we first optimized a bioink for the digital light processing (DLP) printing process and fabricated hepatic tissue constructs using the optimized bioink system. Subsequently, the printed hepatic tissue constructs were integrated with a perfusion system and assessed for tissue survival, phenotypic expression, and hepatic functions.

2. Methods and methods

2.1. Materials

Poly(ethylene glycol)-diacrylate (PEG-DA) with molecular weights of 1 kDa and 4 kDa, 4-arm-PEG acrylate (PEG-A) with molecular weights of 10 kDa and 20 kDa, and 8-arm-PEG-A with molecular weights of 10 kDa and 40 kDa were procured from Creative PEGWorks (Durham, NC). Lithium phenyl(2,4,6-trimethyl benzoyl)phosphinate (LAP) was obtained from Tokyo Chemical Industry (Tokyo, Japan), and 2,2′-Dihydroxy-4,4′-dimethoxybenzophenone-5,5′-bis(sodium sulfonate) (Maxguard R1800) was purchased from Lycus LTD (El Dorado, AR). Gelatin methacryloyl (GelMA) was synthesized by dissolving type A gelatin (~300 g bloom) in CB buffer (0.25 M buffer comprising 7.95 mg/mL sodium carbonate and 0.73 mg/mL sodium bicarbonate in 1 L distilled water), as described in our previous work. Methacrylic anhydride (MAA) was then added to the gelatin solution, and the reaction was allowed to proceed for 3 h. The degree of methacrylate (%) of the GelMA was measured by ^{1}H NMR spectroscopy. All chemicals were purchased from Millipore Sigma (St. Louis, MO), unless otherwise indicated.

2.2. Cell culture

Human hepatocellular carcinoma cell line (HepG2) was obtained from the American Type Culture Collection (ATCC, Manassas, VA) and expanded in 225 cm^2 cell culture flasks until 80 % confluence was achieved with Dulbecco's Modified Eagle's Medium (DMEM, high glucose). The medium was supplemented with 10 % fetal bovine serum (FBS) and 1 % antibiotic/antimycotic. The cells were incubated in 5 % CO_2 at 37°C and were changed with fresh media every 3 days. Human umbilical vein endothelial cells (HUVECs) were cultured in EGM-2 (Lonza, Morrisville, NC) complete medium containing 2 % (v/v) fetal bovine serum (FBS), multiple recombinant human growth factors including vascular endothelial growth factor (VEGF), fibroblast growth factor (FGF), insulin growth factor-1 (IGF-1), and epidermal growth factor, as well as hydrocortisone, heparin, and ascorbic acid. The culture medium was changed every 3 days, and the cells were incubated in 5 % CO_2 at 37°C. All cell culture-related agents were purchased from HyClone (Logan, UT) unless otherwise indicated.

2.3. Construct design and fabrication

ABAQUS/Standard® 6.13 finite element (FEM) software (Simulia, Dassault Systems, Waltham, MA) was employed to simulate the flow dynamics within the designed hepatic tissue constructs. In the preprocessing stage, the 3D CAD models of the gyroid and lattice structures were imported into the software as continuous entities for analysis.

The 3D CAD models of the gyroid and lattice structures were designed using SolidWorks® and exported as a stereolithography (STL) file. Both gyroid and lattice structures, each measuring $1 \times 1 \times 1$ cm^3,

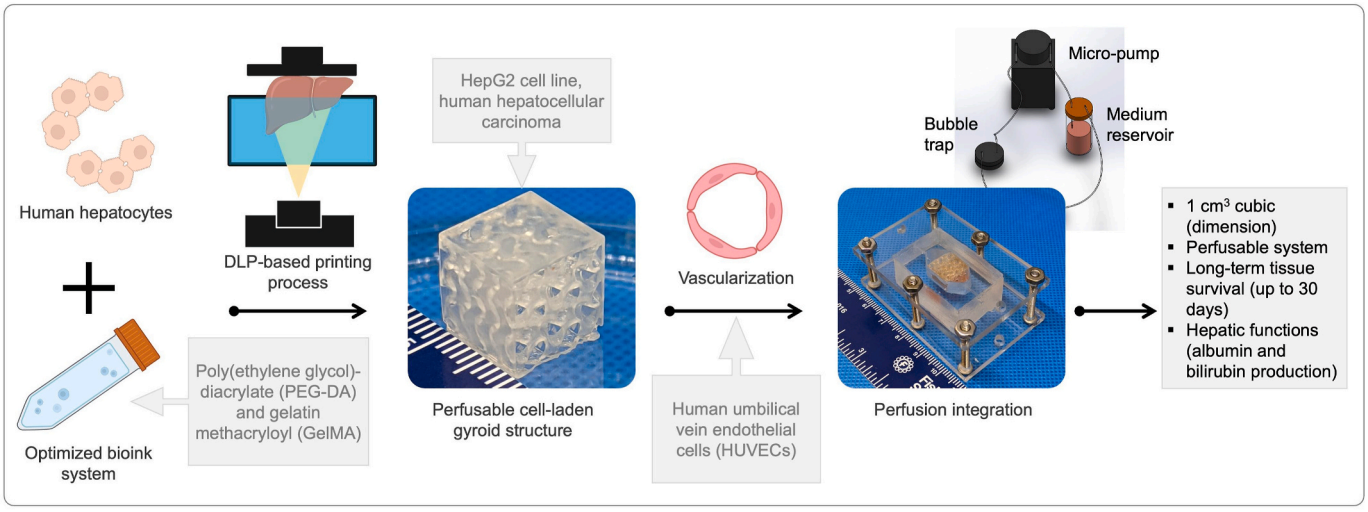

Fig. 1. Schematic illustration of the fabrication process for perfusable, large-scale hepatic tissue constructs ($1 \times 1 \times 1$ cm^3) containing hepatocytes and endothelial cells (ECs) using a digital light processing (DLP) bioprinting technique. The bioprinted hepatic construct is integrated with a perfusion bioreactor system, providing physiologically relevant conditions.

were enclosed within solid outer layers, with openings retained on the inlet and outlet sides to facilitate integration with the perfusion bioreactor system. The cell-laden hydrogel constructs had a volume of 209.59 mm^3 for the gyroid structure and 213.98 mm^3 for the lattice structure. A detailed comparison of these constructs is provided in Table 1. The STL file was sliced along the Z-axis, and each layer was projected using a DLP system to fabricate the designed 3D structure. To ensure sterility, components of the DLP printer susceptible to contamination, such as the stage and vat, were thoroughly sterilized prior to printing.

DLP bioinks were formulated by combining GelMA with PEGs. The concentration of GelMA was maintained at 2 wt% across all bioink formulations, while various types of PEG polymers were incorporated at a concentration of 5 wt%. The formulations were dissolved in phenol-free DMEM supplemented with 0.2 wt% LAP and 0.05 wt% Maxguard R1800 (UV absorber). The solution was stirred for 1 h at 40 °C and filtered through a 0.45-μm syringe filter. HepG2 cells were resuspended in the bioink at 10×10^6 cells/mL.

A total of 11 mL of cell-laden bioink was loaded into the vat for fabrication. DLP printer (Miicraft, Jena, Germany) was conducted by sequentially projecting images of each layer onto the bioink and raising the Z-stage incrementally. The printing parameters were set to a 50-μm layer thickness and 40 s of curing time per layer. Six cell-laden gyroid constructs ($1 \times 1 \times 1$ cm^3) were printed simultaneously, each consisting of 200 layers. The total fabrication time was 187 min. Following fabrication, the constructs were briefly rinsed with media to remove residual bioink and then immersed in fresh media for further processing.

2.4. Optimization of PEG/GelMA bioink formulation for the DLP process

To optimize the PEG/GelMA bioink formulation for the DLP printing process, various PEG polymers with different arm numbers and molecular weights were combined with 2 wt% GelMA. These formulations were systematically evaluated for compressive mechanical properties, printing accuracy, and dimensional stability.

The compressive mechanical properties of the PEG/GelMA constructs were evaluated using an Instron Universal Testing System (Model #5544, Instron Corporation, Issaquah, WA) equipped with a 100 N load cell. Testing was performed at a crosshead speed of 1 mm/min until 25 % compressive strain was achieved. The compressive modulus (Young's modulus) was determined using Equation (1), where E is Young's modulus, σ is stress, and ε is a strain.

$$E = \frac{\sigma(\varepsilon)}{\varepsilon} \quad (1)$$

Printing accuracy was evaluated by determining the percentage deviation between the intended design dimensions and the actual dimensions of the printed PEG/GelMA constructs. To assess dimensional stability in aqueous conditions, the printed PEG/GelMA constructs were immersed in PBS, and changes in their dimensions (swelling ratio) were monitored after 24 h.

2.5. Cell viability and ATP activity

The cell viability of the cell-laden PEG/GelMA constructs was assessed using a Live/Dead® staining assay kit. Live/Dead® analysis was performed employing a calcein-ethidium stain. The calcein-Am (green) component indicates intracellular esterase activity, characteristic of living cells, while the ethidium homodimer-1 (red) component signifies a disruption of plasma membrane integrity. A solution comprising 0.5 μl/mL calcein (4 mM) and 1 μL/mL ethidium (2 mM) in PBS was prepared. Subsequently, the constructs were incubated in this solution for 30 min, shielded from light, and imaged using a Leica Macro-Confocal microscope (Nussloch, Germany). These images were exported as TIF files, which were subsequently analyzed to quantify the percentage of cellular viability.

The ATP activity in the cell-laden PEG/GelMA constructs was assessed using the CellTiter-Glo® Luminescent Assay (Promega, Madison, WI). The constructs were rinsed with sterile PBS, and an ATP assay reagent was added to ensure complete lysis and ATP release. After a 10-min incubation at room temperature, the luminescence was measured using a plate reader. ATP content was quantified by comparing luminescence values to a standard curve prepared with known ATP concentrations, measuring cellular metabolic activity.

Table 1
Comparison of gyroid and lattice constructs ($1 \times 1 \times 1$ cm^3 dimension): porosity, wall thickness, surface area, and channel size.

	Gyroid	Lattice
Volume (mm^3)	209.59	213.98
Porosity (%)	76.3	75.7
Wall thickness (μm)	300	730
Surface area (mm^2)	1490	1170
Channel size (mm)	1.7	1.3

2.6. Perfusion set-up

The perfusion system comprised a flow chamber, bubble trap, medium reservoir, tubing, and micro-pump. Flow chambers for this trial were constructed using a silicone spacer with a 1 cm square recess in the center and attachment points for tubing on both sides of the recess. The constructs were aligned to ensure that the two open faces were parallel to the inlet/outlet, and the closed walls were aligned with the solid silicone walls of the recess. Acrylic sheets were employed to seal the system by placing a solid piece on the open face of the silicone mold and securing it with six bolts to create a watertight seal. Tubing was connected at the inlet/outlet to facilitate media flow. Perfusion was established by pumping media from the reservoir through the bubble trap, through the sample, and back to the reservoir via a peristaltic pump (Elemental Scientific Inc., Omaha, NE). The flow rate was set to 100 μL/min, and the total medium volume contained in the perfusion system was 6 mL.

2.7. Immunofluorescent analysis

The constructs were fixed in 10 % neutral buffered formalin (NBF) overnight at 4 °C. Subsequently, they were permeabilized with 0.2 % (v/v) Triton X-100 for 2 h. The sectioned samples were stained with antibodies against hepatocyte nuclear factor 4-α (HNF4A, 1:200, Abcam), albumin (1:200, Thermofisher), bilirubin (1:200, Biomatik), and von Willebrand factor (vWF, 1:400, Aligent). Nuclei were counterstained with DAPI, and the resulting images were acquired using fluorescence microscopy (BX63 microscope; Olympus, Tokyo, Japan).

2.8. Hepatic function measurement

Albumin was measured using Human Albumin SimpleStep ELISA Kits (ab227933, Abcam, Cambridge, UK). Media was reserved from each media change and frozen until the assay was performed. Then, 50 μL of the sample was assayed according to the kit protocol and compared to a standard curve to calculate the albumin concentration in the sample. All samples were measured using a plate reader (SpectraMax M5, Molecular Devices, San Jose, CA).

Bilirubin concentrations were assayed using a colorimetric assay kit for total and direct bilirubin (ab235627, Abcam). 50 μL of media, reserved from media changes, was reacted with a reagent mix and measured for endpoint absorbance using the plate reader. A standard curve was used to calculate the amount of bilirubin per assay well (μg/well), which was then converted to μg/mL.

2.9. Vascularized hepatic tissue construct

To fabricate vascularized hepatic tissue constructs, HUVECs were seeded onto the printed hepatic constructs at a density of 2×10^6 cells. Subsequently, the constructs were incubated in a 5 % CO_2 atmosphere at 37 °C for 3 h. Following this initial incubation, the constructs were flipped, an additional 2×10^6 cells were seeded on the opposite side, and the construct were incubated for another 3 h. Following seeding, the constructs were integrated into a perfusion system, which was maintained throughout the study. A 1:1 mixture of HepG2 medium (DMEM high glucose supplemented with 10 % FBS and 1 % antibiotic-antimycotic) and EGM-2 complete medium was used. A total of 6 mL of co-culture medium was replaced every 3 days during perfusion. The vascularized hepatic tissue constructs were evaluated by assessing cell viability, cellular morphology, phenotypic expression, and hepatic functions, as described above.

2.10. Statistical analysis

Statistical analysis and quantification of data collected from Live/Dead® staining assay, ATP assay, and functional assays were performed using GraphPad Prism software. All data are presented as mean ± standard deviation from our experimental samples. Statistical significance was assessed using a two-way ANOVA with multiple comparisons. $P < 0.05$ was considered statistically significant.

3. Results

3.1. Optimized bioink formulation for the DLP process

To optimize the bioink formulation for DLP-based fabrication of hepatic tissue constructs, a series of PEG polymers with varying numbers of arms and molecular weights were combined with GelMA. Among these formulations, the 10 kDa 4-arm PEG-A demonstrated the highest compression modulus compared to the other formulations (Fig. 2A and B). Printing accuracy was assessed by comparing the designed printing resolution with the actual printed resolution. The 10 kDa 4-arm PEG-A exhibited superior printing accuracy (Fig. 2C). Dimensional stability was evaluated through swelling ratio measurements. The results showed that the 10 kDa and 20 kDa 4-arm PEG-As, along with the 10 kDa and 40 kDa 8-arm PEG-As, had swelling ratios below 10 %, indicating minimal dimensional changes in aqueous environments (Fig. 2D).

To evaluate the biological properties of the PEG/GelMA-based bioink formulations, HepG2 cells were DLP-printed using various PEG/GelMAformulations. Live/Dead® staining confirmed that none of the formulations compromised cell viability within the printed constructs (Fig. 2E). Moreover, cells demonstrated self-assembly behavior, forming aggregates in the 4 kDa PEG-DA and 10 kDa 4-arm PEG-A formulations. ATP assays further indicated cellular proliferation over time in the printed constructs, except for those fabricated with 1 kDa PEG-DA and 10 kDa 8-arm PEG-A (Fig. 2F).

Based on the results, the 10 kDa 4-arm PEG-A and GelMA formulation was selected as the DLP bioink for subsequent experiments. This formulation demonstrated the capability to fabricate diverse construct shapes with high resolution using the DLP process (Fig. 2G).

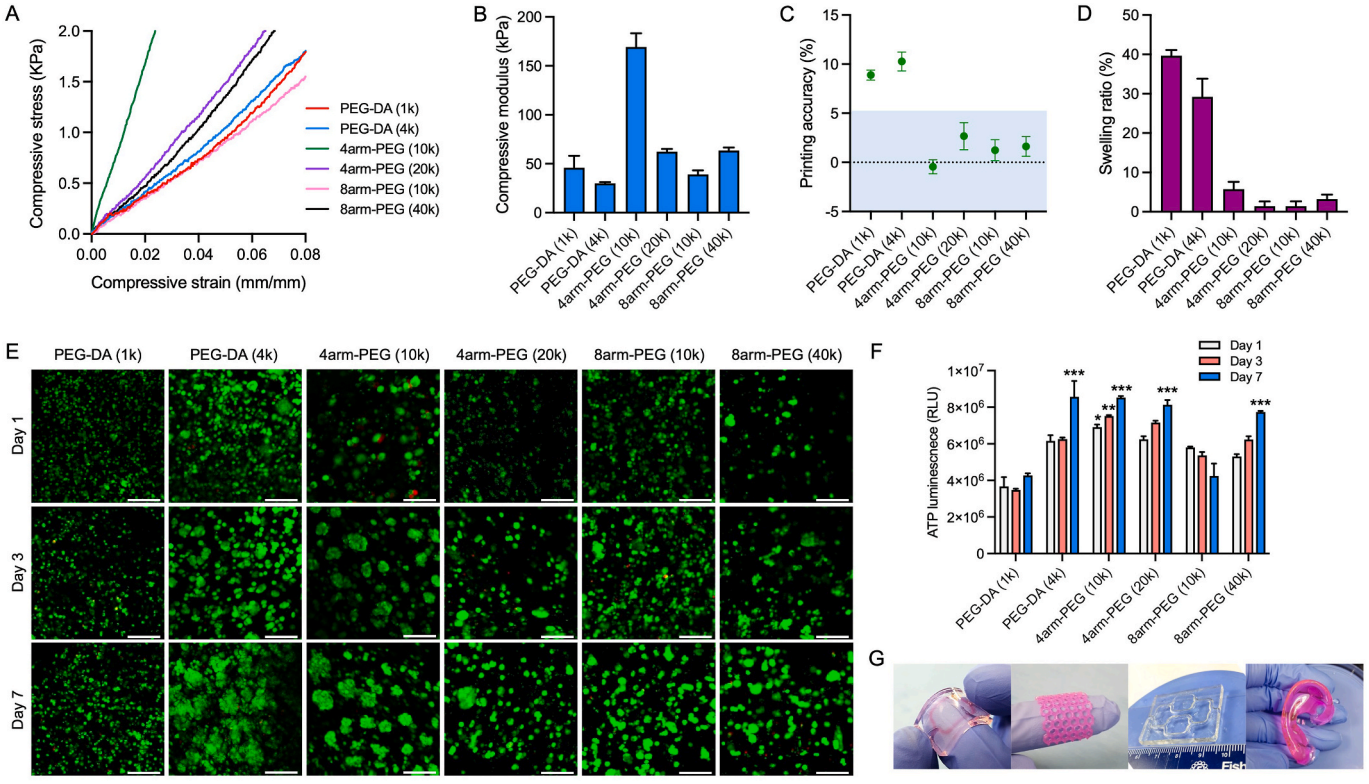

Fig. 2. Optimization of PEG/GelMA composite bioink formulations with various PEG types (diacrylate, 4-arm, and 8-arm) and molecular weights. (A) Compressive stress-strain curves and (B) compressive modulus values demonstrate mechanical properties of the bioinks (n = 5). (C) Printing accuracy (%) comparing printed resolution to the designed resolution (n = 5). (D) Swelling ratio (%) showing dimensional changes after 24 h in aqueous conditions (n = 5). (E) Live/dead staining images of printed constructs containing HepG2 cells for various PEG/GelMA formulations. (F) ATP activity analysis to assess the metabolic activity (n = 5). *$P < 0.05$ compared with other groups at Day 1, **$P < 0.05$ compared with other groups at Day 3, and ***$P < 0.05$ compared with other groups at Day 7. (G) The 4-arm PEG (10k)/GelMA composite bioink achieves the best printing outcomes, demonstrated by diverse construct shapes, including 2-channel, meshed, multi-channel, and ear-shaped designs. All data are represented as mean ± SD.

3.2. FEM simulation and construct fabrication

Based on FEM simulation results, the gyroid-shaped architecture effectively distributed uniform flow and surface shear stress across the entire inner surfaces of cell-laden tissue constructs. This design strategy ensures a consistent supply of oxygen and nutrients to cells within the construct during perfusion. The targeted construct had dimensions of 1 × 1 × 1 cm^3, with 76.3 % of the porosity of the gyroid constructs (Table 1). The simulation results were validated, confirming the absence of vortex formation and the consistent application of shear stress to all channels at a flow rate of 100 μL/min (Fig. 3A). Particularly, the gyroid structure showed uniform surface shear stress up to 300 μL/min flow rate (Supplementary Fig. 1). In contrast to the gyroid structure, the lattice structure (75.7 % porosity) exhibited challenges in achieving uniform flow and surface shear stress distribution. The lattice structure revealed a high surface shear stress distribution.

Using the DLP process, the PEG/GelMA composite bioink was utilized to fabricate cell-laden gyroid constructs. The gyroid constructs (1 × 1 × 1 cm^3) containing 10 × 10^6 cells/mL of HepG2 cells were successfully fabricated.

3.3. Gyroid vs. lattice structures

To validate the gyroid structure under perfusion conditions, cell-

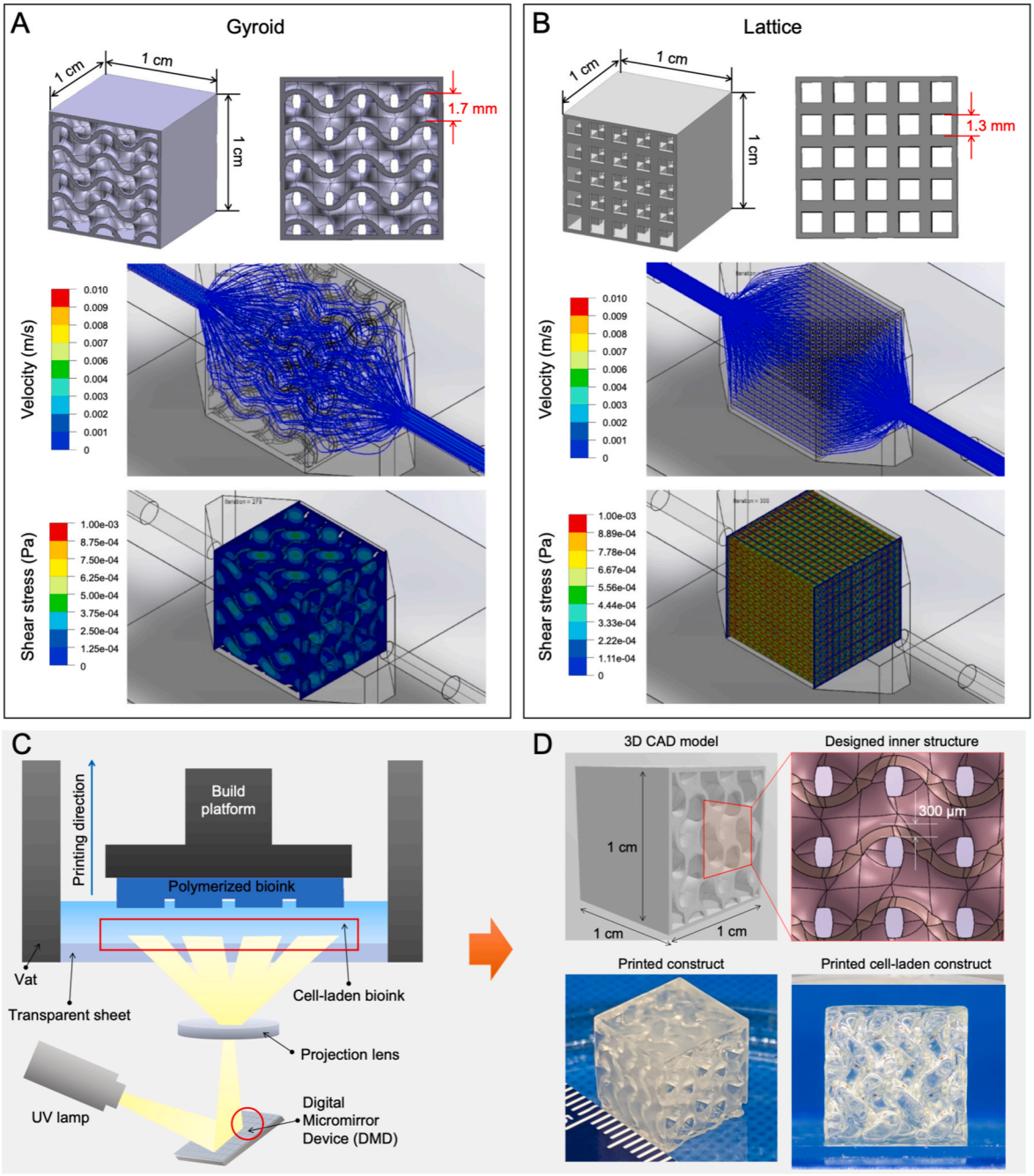

Fig. 3. Design strategy and fabrication of perfusable hepatic tissue constructs. 3D CAD design and FEM simulation comparing (A) gyroid-shaped and (B) lattice constructs, highlighting uniform fluid flow (flow rate and surface shear stress) in the gyroid-shaped design at a flow rate of 100 μL/min. (C) Schematic illustration of the DLP bioprinting process. (D) CAD model and cross-sectional view of the gyroid-shaped construct, showing a uniform wall thickness of 300 μm. The cell-laden constructs were fabricated using the DLP bioprinting technique.

laden constructs with gyroid and lattice structures were cultured under static and perfusion conditions. Live/Dead® staining of the constructs was performed on days 0, 10, and 20. The samples were observed in three distinct construct regions: inlet, middle, and outlet (Fig. 4A). Immediately after printing, most cells exhibited uniformly distributed viable cells (green), with only a few dead cells (red). After 10 days in culture, the samples showed more aggregated cells than the day 0 samples, indicating active cellular proliferation under static and perfusion conditions (no significant difference at 10 days in culture) (Fig. 4B and C). Live/Dead staining revealed >90 % cell viability at days 0 and 10. However, the gyroid constructs under perfusion exhibited higher cell viability compared to both lattice and gyroid constructs under static conditions at day 20 in culture (Fig. 4B and C). Although the gyroid construct under perfusion exhibited slightly higher cell viability than the lattice construct under perfusion, there was no statistically significant difference.

Cellular function was confirmed by immunofluorescent staining of albumin and bilirubin. Notably, HepG2 cells in the gyroid construct under perfusion conditions exhibited enhanced cellular organization (Fig. 5A). Furthermore, distinct aggregates were observed at day 10, which progressively expanded and matured throughout day 20. These findings revealed a substantial disparity between the gyroid perfusion group and both static and perfusion lattice groups, indicating a higher level of hepatic function within the perfusion group.

The hepatic tissue constructs demonstrated the capacity to produce physiologically relevant levels of albumin, urea and bilirubin throughout the 20-day duration (Fig. 5B–D). At day 20, the gyroid constructs under perfusion conditions exhibited significantly elevated levels of albumin and bilirubin compared to lattice and gyroid groups under static conditions. Despite the gyroid constructs exhibiting slightly higher values than the lattice constructs under perfusion conditions, no statistically significant difference was observed. While both perfusion groups demonstrated increased hepatocyte aggregation and functional expression, the unique gyroid design demonstrated the ability to produce elevated levels of albumin and bilirubin to a statistically significant extent. These findings establish a correlation between the increased aggregation observed in the perfusion groups and the enhanced functionality of the hepatic tissue constructs.

3.4. Vascularized hepatic tissue construct

To develop the vascularized hepatic tissue construct, HUVECs were successfully seeded into the hepatic gyroid constructs. These constructs were subsequently integrated with the perfusion system (Fig. 6A). Continuous perfusion was maintained throughout the constructs without evidence of uncontrolled leakage for the entire trial duration (Supplementary Figure 2), and the original dimension of the constructs was also maintained during the 30-day perfusion period (Supplementary Figure 3).

Live/Dead® staining of the vascularized hepatic tissue constructs under perfusion on days 10, 20, and 30) was performed. The samples were examined in three distinct construct regions: inlet, middle, and outlet (Supplementary Figs. 4, 5, and 6). The majority of cells exhibited uniformly distributed viable cells (green), with only a few dead cells (red) (Fig. 6B). After 10 days of culture, the samples exhibited a higher density of aggregated cells compared to the day 0 samples, indicating an active cellular proliferation under perfusion. The 3D-rendered images of various planes revealed aggregated cells, which are highly probable to be hepatocytes. Quantitatively, >85 % cell viability was presented at all time points under perfusion; on days 0, 10, 20, and 30 (Fig. 6C). Cell viability is maintained by nutrient delivery through the perfusion of tissue constructs without any external support during the 30-day trial. During perfusion, HepG2 cells settled and self-aggregated to form cell clusters. These gradually formed well-defined cell aggregates over 30 days. The cell size distribution showed a wide range of sizes, likely due to the increased aggregation of hepatocytes over time (Fig. 6D).

Cell proliferation was confirmed by Ki67 immunofluorescent staining. Proliferation was prominent (Ki67-expressed, green) in the aggregated cells (hepatocytes) (Supplementary Figure 7A). Furthermore, the cell proliferation in the tissue constructs was determined by the luminescent ATP Detection Assay Kit. The ATP assay confirmed that the cells within the samples are metabolically active (Supplementary Figure 7B). The results showed that the ATP level of the day 20 samples was significantly higher than that of the day 10 samples, and the day 30 sample was slightly lower compared with the day 20 samples (Supplementary Fig. 7C). These findings may be attributed to the high cell confluence within the limited space in the construct.

To confirm the hepatic phenotypes, the constructs were co-stained

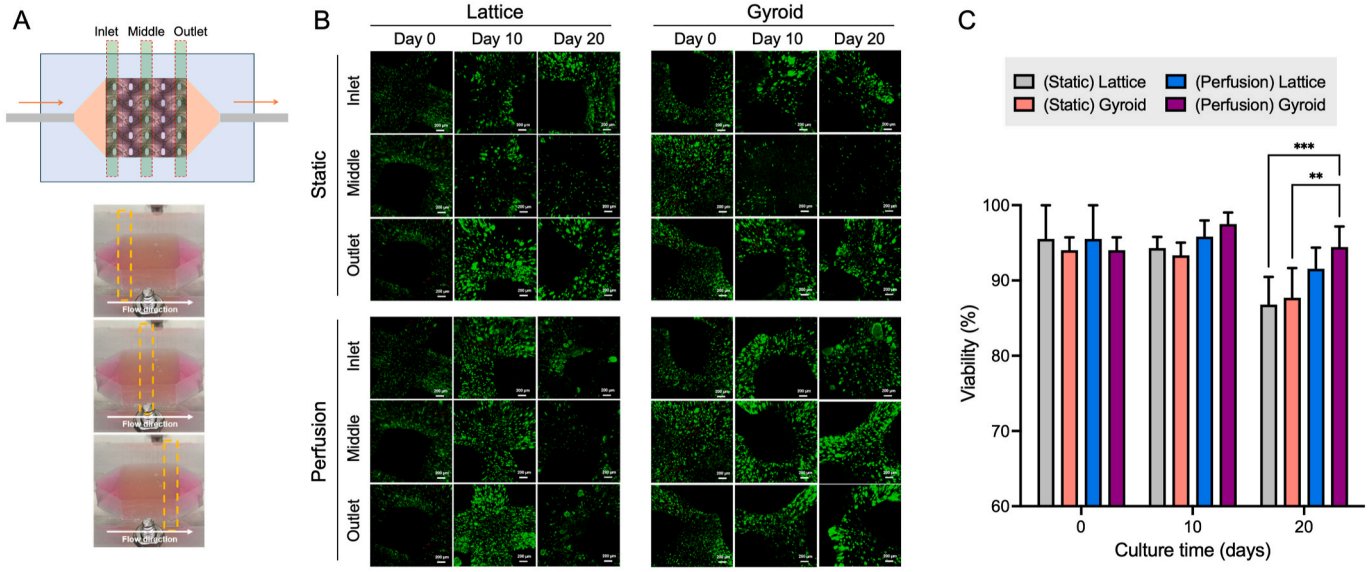

Fig. 4. Cell viability analysis of the printed hepatic constructs. (A) The hepatic constructs were segmented into three regions: inlet, middle, and outlet for analysis. (B) Live/dead staining images of lattice and gyroid constructs under static and perfusion conditions at 0, 10 and 20 days. (C) Quantified cell viability (%) based on live and dead cells within the printed constructs (n = 5). $^{**}P < 0.05$, $^{***}P < 0.01$. All data are represented as mean ± SD. The *P*-values by a two-way ANOVA with multiple comparisons are indicated.

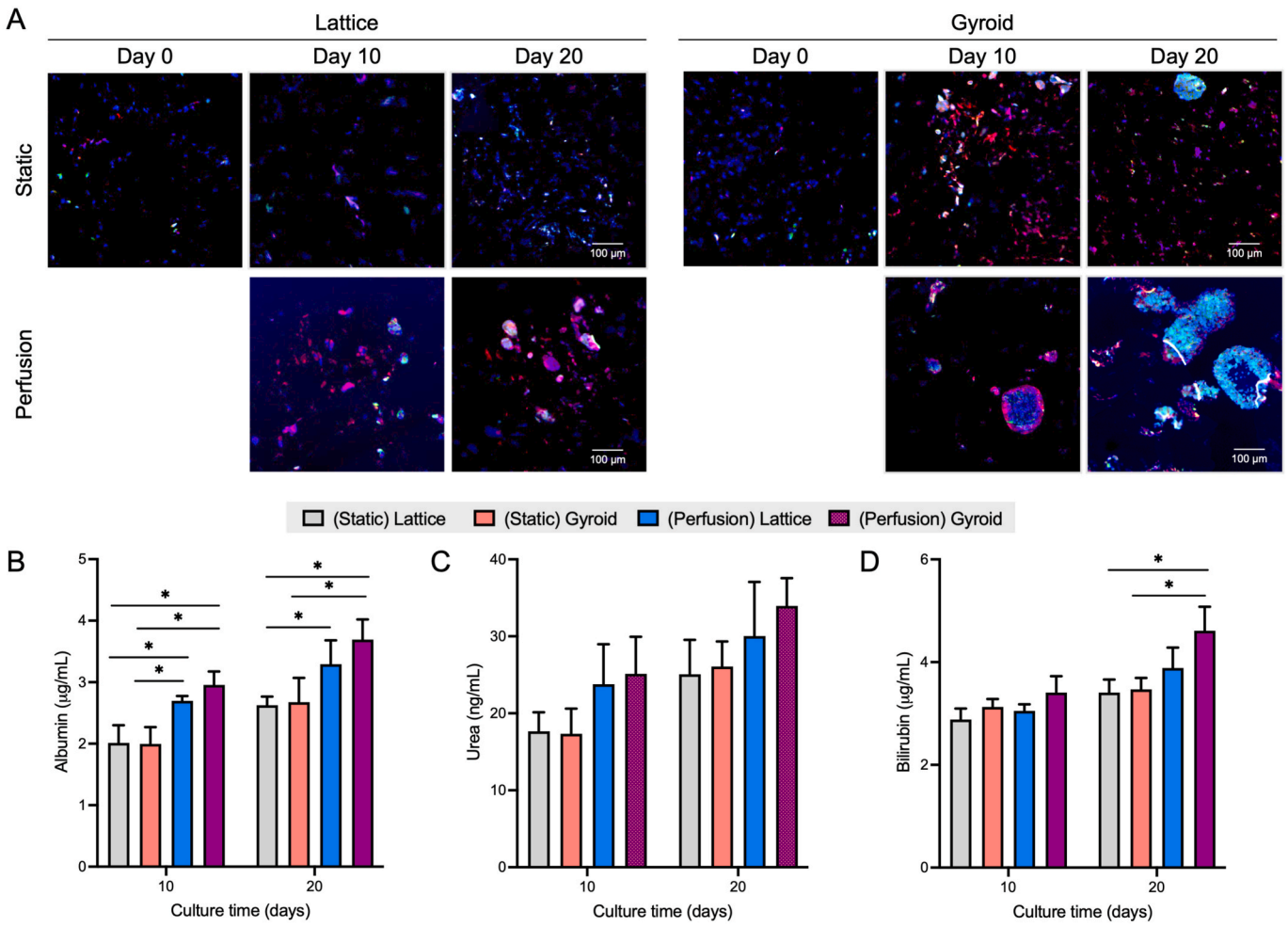

Fig. 5. Hepatic cell phenotype and function. (A) Immunofluorescent staining of printed hepatic constructs for albumin and bilirubin at days 0, 10, and 20. Albumin (red), bilirubin (green), and DAPI (blue). (B) Quantification of albumin production (n = 6). (C) Quantification of urea production (n = 6). (D) Quantification of bilirubin production (n = 6). $^{**}P < 0.05$. All data are represented as mean ± SD. The *P*-values by a two-way ANOVA with multiple comparisons are indicated. (For interpretation of the references to color in this figure legend, the reader is referred to the Web version of this article.)

with HNF4A and albumin. HNF4A-positive cells within the constructs indicate aggregated hepatocytes. Hepatocytes were further confirmed by HNF4A and albumin (Fig. 7A). Single hepatocytes (green) at day 0 transformed into aggregated morphology at day 10, accompanied by albumin expression (red). The day 20 and day 30 samples consistently exhibited expression of the hepatocyte-specific antibodies (HNF4A, green) and albumin (red). Endothelial cells were confirmed by endothelial cell-specific antibodies (vWF). The endothelial cells (red) are uniformly distributed throughout the construct. The day 20 and day 30 samples clearly demonstrate an endothelial layer covering the lumen of the construct, with viable hepatocyte aggregates present within the construct's interior region. This observation was confirmed by double staining with vWF (red; endothelial cells) and DAPI (blue; hepatocytes) (Fig. 7B). This finding suggests that the viability of hepatocytes is maintained by perfusate diffusion, which provides essential nutrients and oxygen. This demonstrates the functional capacity of the endothelial cells within the vascularized construct. (L: lumen of the vascular channel).

Quantitative analysis of albumin and bilirubin production was performed using media collected throughout the 30-day perfusion period. The perfusate from samples collected at various time points consistently demonstrated albumin production. Notably, the accumulated total albumin produced over 21 days of perfusion reached approximately 110 μg, a level comparable to that found in human blood (Fig. 7C). Similarly, the total bilirubin in the collected media revealed continuous production by the bioprinted tissue constructs during the 30-day perfusion period (Fig. 7D). The bilirubin concentration ranged from 1 to 6 μg/mL across the time points, aligning with levels observed in human blood, indicating sustained functionality of the hepatocytes within the constructs.

4. Discussion

To fabricate vascularized liver tissue, a study developed a 3D liver model incorporating branched vascular networks to enhance perfusion [20]. However, limitations in nutrient and oxygen diffusion persist in regions of the construct due to the inherent properties of hydrogel-based materials. Another investigation utilized 3D bioprinted microgels to create implantable vascularized tissues [23], which similarly experienced inadequate nutrient and oxygen delivery, resulting in non-perfused areas. Volumetric bioprinting of organoids using optically tunable hydrogels has demonstrated potential in generating liver-like metabolic biofactories [24]. This study explored the flow characteristics of three triply periodic minimal surface (TPMS) geometries. The evaluation involved measuring albumin and GLDH levels after 24 h of perfusion. Although these findings suggest the constructs could serve as *in vitro* liver models, the study did not assess their long-term functionality or physiological relevance to human liver tissue. In our study, we assessed hepatocyte function and maturity over a 30-day period by quantifying key hepatic markers, including albumin and bilirubin production.

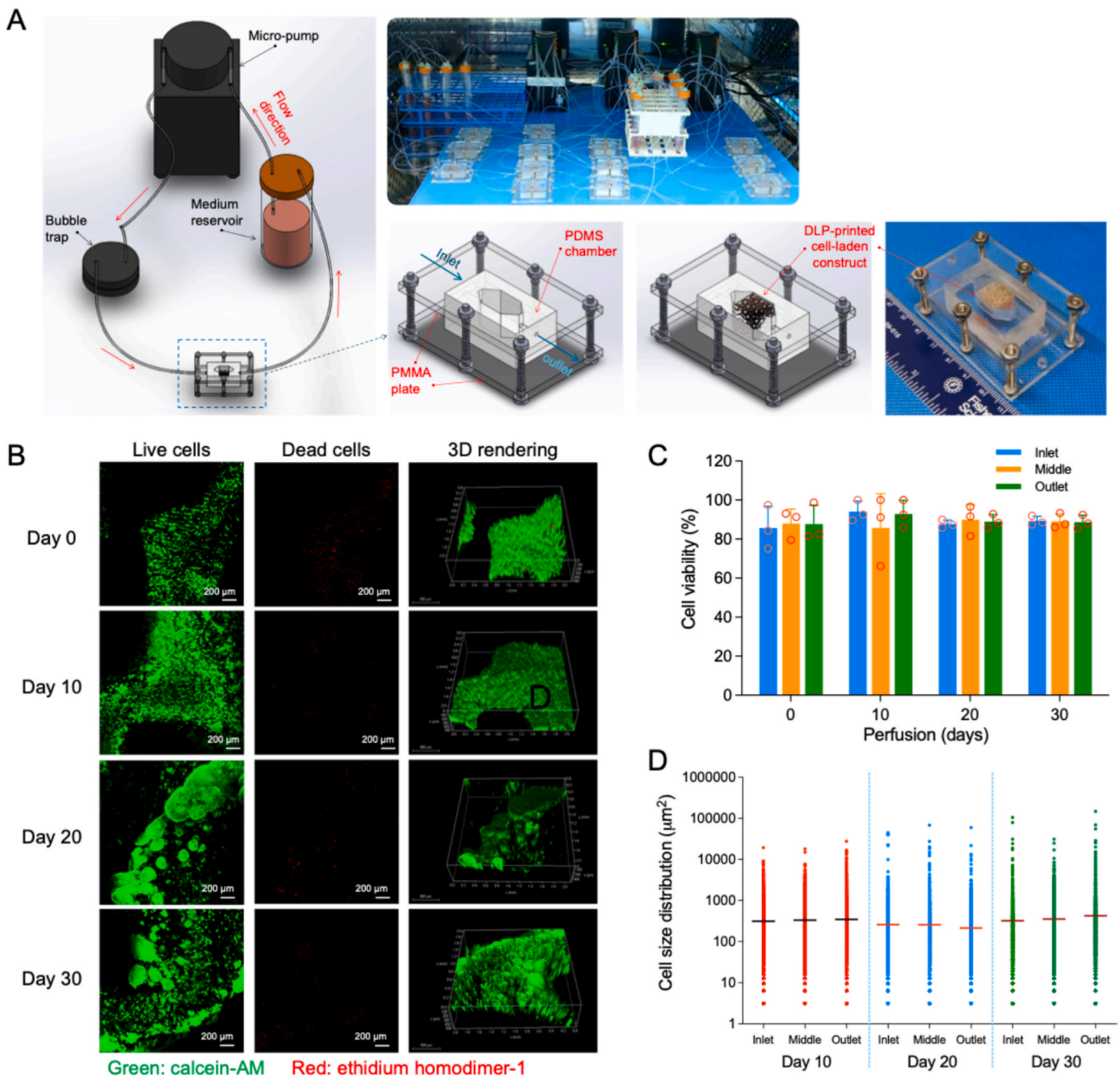

Fig. 6. Vascularized hepatic tissue constructs. (A) Schematic illustration and photograph of the perfusion system for DLP-printed gyroid hepatic constructs containing HepG2 cells and ECs. The liver constructs were positioned in a PDMS flow chamber for perfusion. (B) Live/Dead staining images of the hepatic constructs over the 30-day perfusion period. (C) Quantification of cell viability (%) in different regions of the constructs during the 30-day perfusion (n = 3). (D) Cell size distribution in various regions of the constructs throughout the 30-day perfusion (n = 3). All data are represented as mean ± SD. The p-values by a two-way ANOVA with multiple comparisons are indicated.

This study presents a novel approach to fabricating vascularized large tissue constructs that maintain cellular viability and metabolic function for a prolonged period. Motivated by the NASA Vascular Tissue Challenge [25], which is part of the Centennial Challenges program, this study addresses the continued challenge associated with vascularization of tissue-engineered organ constructs. The challenge required the development of a vascularized human organ construct (1 cm^3) integrated with active perfusion for a 30-day trial. In this challenge, we took an approach of bioprinting vascularized liver tissue constructs by incorporating human hepatocytes and ECs. The constructs were evaluated on their ability to maintain over 85 % cell viability and demonstrate key hepatic functions, including albumin and bilirubin production. We utilized the gyroid design to provide evenly distributed active perfusion to the hepatic tissue construct. This design ensures uniform flow and low shear stress across the inner surfaces of the cell-laden tissue constructs, facilitating a consistent supply of oxygen and nutrients to the cells within the construct. **Supplementary Video** provides a comprehensive overview of the entire process, encompassing bioink preparation, DLP bioprinting, and perfusion procedure.

In this study, we utilized a composite bioink system comprising PEG and GelMA. PEG was hypothesized to contribute suitable mechanical properties and printing precision, while GelMA was expected to enhance

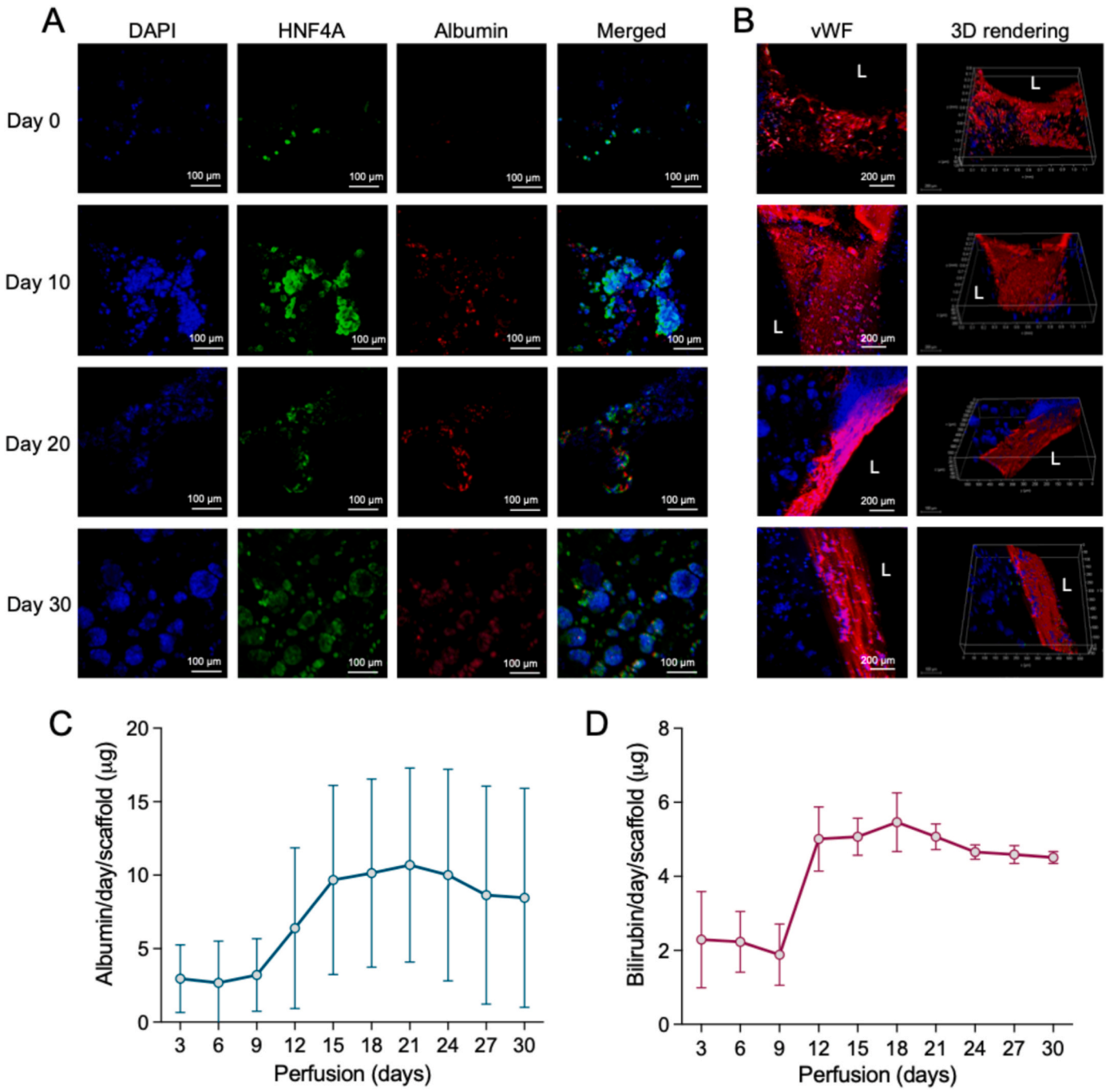

Fig. 7. Cell phenotype and hepatic functions. (A) Immunofluorescent staining for HNF4A (green) and albumin (red) in vascularized hepatic tissue constructs at days 0, 10, 20, and 30 post-perfusion. (B) Immunofluorescent staining for vWF (red) and DAPI (blue) in vascular tissue constructs at days 0, 10, 20, and 30 post-perfusion. L: Lumen. (C) Total albumin production per day per scaffold during the 30-day perfusion: days 3, 6, 9 (n = 15); days 12, 15, 18, 21 (n = 10); days 24, 27, 30 (n = 5). (D) Quantification of bilirubin production from the printed hepatic constructs during the 30-day perfusion: days 3, 6, 9 (n = 15); days 12, 15, 18, 21 (n = 10); days 24, 27, 30 (n = 5). All data are represented as mean ± SD. (For interpretation of the references to color in this figure legend, the reader is referred to the Web version of this article.)

biological compatibility, supporting tissue-specific cell types [26]. To optimize the bioink formulation for the DLP printing process, various PEG polymers were combined with GelMA. The PEG/GelMA composite bioinks demonstrated distinct mechanical properties, printing accuracy, and dimensional stability depending on the number of arms and molecular weights of the PEG polymers. Compression testing confirmed the mechanical properties of each formulation and its suitability for the printing process. In hydrogel-based constructs, enhanced mechanical strength is particularly advantageous for DLP-based bioprinting, which depends on a layer-by-layer fabrication strategy. For successful 3D construct formation, each printed layer must retain sufficient structural integrity to support the subsequent layers during printing. High printing accuracy is also critical for fabricating complex geometries, such as gyroid structures. Furthermore, dimensional stability - specifically, resistance to swelling or deformation - is essential for maintaining construct integrity during long-term perfusion culture. Based on these criteria, the optimized bioink formulation consisting of 5 wt% 10 kDa PEG-A and 2 wt% GelMA, exhibited outstanding mechanical properties,

printing precision, dimensional stability, and biological compatibility.

This study emphasized the critical role of efficient fluid dynamics in engineered tissue constructs and demonstrated the effectiveness of gyroid-shaped architectures in overcoming challenges associated with functional vasculature fabrication. The gyroid structure, characterized by its interconnected channels [27], promotes uniform fluid flow and optimal surface shear stress, enhancing nutrient and oxygen distribution throughout the cell-laden construct. In our construct design, the channel size (1.7 mm) in the gyroid-shaped architecture was determined based on the wall thickness, which was set at 300 μm. This value was chosen to exceed the typical diffusion limit of hydrogel-based constructs (~200 μm) [28], ensuring sufficient nutrient and oxygen transport to the encapsulated cells. To compare two different construct designs, we ensured that the gyroid and lattice structures had closely matched volume (mm^3) and porosity (%) in our experiments. Our results demonstrate that gyroid-shaped constructs achieved a more uniform cell distribution under perfusion conditions compared to lattice constructs. These findings align with FEM simulations, which predicted higher surface shear stress and irregular flow rates in lattice structures.

Both gyroid and lattice constructs showed improved cellular distribution under perfusion compared to static conditions. However, gyroid constructs outperformed lattice constructs by achieving more uniform cell distribution and higher cell viability after 20 days in culture. While lattice constructs under perfusion conditions also enhanced cellular distribution, the elevated shear stress in these constructs led to lower albumin and bilirubin production compared to gyroid constructs. This highlights the importance of balancing fluid flow optimization with shear stress minimization, demonstrating the critical need for construct designs tailored to specific applications. Gyroid-shaped constructs provide a promising solution for enhancing cell viability and functionality *in vitro* by effectively mimicking the oxygen and nutrient delivery systems found in living tissues.

A key observation in the vascularized hepatic tissue constructs containing hepatocytes and ECs was the homogeneous cellular distribution and well-defined hepatocyte aggregates within the gyroid constructs under perfusion conditions. The hepatic constructs consistently maintained phenotypic expression of both hepatocytes and ECs. Notably, EC coverage along the luminal surfaces of the constructs remained intact throughout the 30-day trial. Furthermore, the vascularized hepatic constructs produced physiologically relevant levels of albumin and bilirubin (in the microgram range) over the entire trial period. This achievement can be attributed to the large-scale construct (1 cm^3) with uniform cell distribution, maturation, and high cell viability.

While this study offers valuable insights into the potential of 3D printing for hepatic tissue constructs, several limitations warrant consideration for future studies. First, HepG2 cells, a cancerous liver cell line known for their high proliferative capacity and resilience, were utilized in this study. Although this approach facilitated the optimization of design and fabrication parameters, future studies should investigate alternative cell types to develop more physiologically relevant models. Second, the constructs included only HepG2 cells and HUVECs. To create a more comprehensive model, future studies should incorporate additional cell types, such as Kupffer cells, stellate cells, and sinusoidal ECs [29]. While the use of primary liver cells presents challenges related to cell expansion, exploring alternative cell sources, such as stem cells, could help bridge the gap toward clinically relevant models [30, 31]. Despite these limitations, this study demonstrates a robust proof of concept for bioprinting hepatic tissue equivalents. The ability to generate physiologically relevant tissue models holds significant promise for advancing drug screening, personalized medicine, and tissue regeneration therapies.

5. Conclusion

We successfully engineered thick, vascularized human hepatic tissue constructs in an *in vitro* environment, maintaining key metabolic functions comparable to native liver tissue over a 30-day culture period. This was achieved through the development of optimized PEG/GelMA bioink formulations tailored for DLP-based bioprinting. The introduction of a novel gyroid architecture enabled the fabrication of perfusable constructs, supporting uniform cell distribution, enhanced viability, and sustained hepatic functionality under dynamic culture conditions. Moreover, our perfusable hepatic constructs demonstrated albumin and bilirubin production levels comparable to those found in human blood. Our findings highlight the potential of gyroid-structured constructs to advance the field of organ engineering by providing a platform for physiologically relevant, perfusable *in vitro* liver models. Future work should focus on integrating multiple liver-specific cell types, exploring alternative biomaterials, and assessing long-term functionality for applications such as hepatotoxicity testing and drug screening. The innovative application of the gyroid design in this study represents a significant step forward in the development of next-generation vascularized organ models.

CRediT authorship contribution statement

Young-Wook Moon: Writing – original draft, Methodology, Investigation, Formal analysis, Data curation. **Timothy Dobroski:** Writing – original draft, Methodology, Investigation, Formal analysis. **Kelsey Willson:** Methodology, Investigation. **Jin-Oh Jeong:** Writing – original draft, Investigation. **Colin Bishop:** Writing – review & editing, Methodology. **Anthony Atala:** Funding acquisition, Conceptualization. **James J. Yoo:** Writing – review & editing, Resources, Funding acquisition, Conceptualization. **Sang Jin Lee:** Writing – review & editing, Supervision, Resources, Methodology, Funding acquisition, Conceptualization.

Declaration of competing interest

The authors declare that they have no known competing financial interests or personal relationships that could have appeared to influence the work reported in this paper.

Acknowledgment

This study was supported, in part, by NIH/NIBIB (1P41EB023833), Medical Technology Enterprise Consortium (#W81XWH-15-9-0001), and the State of North Carolina (#30962). This project was awarded 1st place in the NASA Vascular Tissue Challenge. The authors would like to thank Dr. Anahita Soufivand for providing the Finite Element Method (FEM) simulation.

Appendix A. Supplementary data

Supplementary data to this article can be found online at https://doi.org/10.1016/j.mtbio.2025.101786.

Data availability

Data will be made available on request.

References

[1] S.J. Lee, et al., Adv. Mater. 36 (49) (2024) e2408032.
[2] A. Atala, Tissue Eng. 30 (1–2) (2024) 5.
[3] L. Somasekhar, L.G. Griffiths, Stem Cells Transl Med 12 (9) (2023) 588.
[4] A.M. Jorgensen, et al., Chem. Rev. 120 (19) (2020) 11093.
[5] F.A.P. Rodrigues, et al., Macromol. Biosci. 24 (12) (2024) e2400139.
[6] J. Fu, D.A. Wang, Trends Biotechnol. 36 (8) (2018) 834.
[7] E.S. Mirdamadi, et al., Tissue Eng., Part B 26 (2) (2020) 145.
[8] H.W. Kang, et al., Nat. Biotechnol. 34 (3) (2016) 312.
[9] A.M. Jorgensen, et al., Sci. Transl. Med. 15 (716) (2023) eadf7547.
[10] S.H. Kim, et al., Biomaterials 258 (2020) 120267.
[11] H. Lee, et al., Adv. Healthcare Mater. 13 (4) (2024) e2302508.

[12] H. Lee, et al., Appl. Phys. Rev. 8 (2) (2021) 021405.
[13] D.O. Visscher, et al., Acta Biomater. 121 (2021) 193.
[14] B. Mahadik, et al., Biofabrication 15 (1) (2022).
[15] C. Bosmans, et al., Trends Biotechnol. 42 (6) (2024) 739.
[16] J. Huh, et al., Tissue Eng. 30 (13–14) (2024) 333.
[17] J.H. Kim, et al., Nat. Commun. 11 (1) (2020) 1025.
[18] D.B. Kolesky, et al., Proc. Natl. Acad. Sci. U. S. A. 113 (12) (2016) 3179.
[19] L.E. Bertassoni, et al., Lab Chip 14 (13) (2014) 2202.
[20] X. Liu, et al., Adv. Healthcare Mater. 10 (23) (2021) e2101405.
[21] A.H. Schoen, Infinite Periodic Minimal Surfaces without Self-Intersections, National Aeronautics and Space Administration, 1970.
[22] A.H. Schoen, Interface focus 2 (5) (2012) 658.
[23] X. Wang, et al., Cell Prolif. 56 (5) (2023) e13456.
[24] P.N. Bernal, et al., Adv. Mater. 34 (15) (2022) e2110054.
[25] Vascular Tissue Challenge. https://www.nasa.gov/prizes-challenges-and-crowdsourcing/centennial-challenges/vascular-tissue-challenge/.
[26] J. Huh, et al., Biofabrication 13 (3) (2021).
[27] S. Seehanam, et al., Heliyon 9 (5) (2023) e15711.
[28] R.K. Jain, et al., Nat. Biotechnol. 23 (7) (2005) 821.
[29] J. Wang, et al., Adv. Healthcare Mater. 13 (21) (2024) e2302217.
[30] J. Guo, et al., Adv. Sci. 8 (10) (2021) 2004680.
[31] D. Bayarsaikhan, et al., Tissue Eng Regen Med. 21 (8) (2024) 1245.